

Prediction of heavy precipitation in the eastern China flooding events of 2016: Added value of convection-permitting simulations

Puxi Li^{1,2}  | Zhun Guo³ | Kalli Furtado⁴ | Haoming Chen⁵ | Jian Li⁵ | Sean Milton⁴ | Paul R. Field^{4,6} | Tianjun Zhou^{1,2}

¹LASG, Institute of Atmospheric Physics, Chinese Academy of Sciences, Beijing, China

²University of Chinese Academy of Sciences, Beijing, China

³Climate Change Research Center, Institute of Atmospheric Physics, Chinese Academy of Sciences, Beijing, China

⁴Met Office, Exeter, UK

⁵Chinese Academy of Meteorological Sciences, China Meteorological Administration, Beijing, China

⁶School of Earth Sciences and the Environment, University of Leeds, Leeds, UK

Correspondence

K. Furtado, Met Office, Exeter, UK.
Email: kalli.furtado@metoffice.gov.uk

Funding information

Climate Science for Service Partnership: China; National Natural Science Foundation of China, 41330423, 41420104006

Abstract

During the period from June 30th to July 6th, 2016, a heavy rainfall event affected the middle and lower reaches of the Yangtze River valley in eastern China. The event was characterized by high-intensity, long-duration (lasted more than 6 days) precipitation and huge amounts (over 600.0 mm) of rainfall. The rainfall moved eastward from the Sichuan basin to the middle Yangtze River valley during the first 2 days, then Mei-yu front formed and circulations became more “quasi-stationary”. During the second-phase, successive heavy rainfall systems occurred repeatedly over the same areas along the front, leading to widespread and catastrophic flooding. In this study, limited-area convection-permitting models (CPMs) covering all of eastern China, and global-model simulations from the Met Office Unified Model are compared to investigate the added values of CPMs on the veracity of short-range predictions of the heavy rainfall event. The results show that all the models can successfully simulate the accumulated amount and the evolution of this heavy rainfall event. However, the global model produces too much light rainfall (10.0 mm/day), fails to simulate the small-scale features of both atmospheric circulations and precipitation, and tends to generate steady heavy rainfall over mountainous region. Afternoon precipitation is also excessively suppressed in global model. By comparison, the CPMs add some value in reproducing the spatial distribution of precipitation, the smaller-scale disturbances within the rain-bands, the diurnal cycle of precipitation and also reduce the spurious topographical rainfall, although there is a tendency for heavy rainfall to be too intense in CPMs.

KEYWORDS

convection permitting model, heavy rainfall, Mei-yu front, prediction, topographical rainfall

1 | INTRODUCTION

The Mei-yu season (the period from mid-June to mid-July) is the second major stationary phase of the summer monsoon in East Asia (Tao, 1987; Ding, 1992; Ding and Chan, 2005;

Zhou *et al.*, 2009; Luo *et al.*, 2013). The Mei-yu season is characterized by the presence, along the middle and lower reaches of the Yangtze River Basin (hereafter YRB-ML), of a subtropical convergence-zone called the Mei-yu front. The front is often identified by sharp meridional gradients in

This is an open access article under the terms of the Creative Commons Attribution License, which permits use, distribution and reproduction in any medium, provided the original work is properly cited.

© 2019 The Authors. *Quarterly Journal of the Royal Meteorological Society* published by John Wiley & Sons Ltd on behalf of the Royal Meteorological Society.

specific humidity and equivalent potential temperature, and as a horizontal wind shear line, but has only a relatively weak temperature gradient in the middle and lower troposphere (i.e., below 500 hPa; Ninomiya, 1984; Wu *et al.*, 2003; Shinoda *et al.*, 2005; Sampe and Xie, 2010; Tomita *et al.*, 2011). The YRB-ML often experiences heavy rainfall due to convective systems that move from west to east along the river valley. Because of its quasi-stationary characteristics, the Mei-yu front can act as a “guide” for these storms, heavy rainfall events often occur and propagate eastward repeatedly in a narrow latitudinal corridor over the YRB-ML (Chen *et al.*, 1998; Ding and Chan, 2005; Ninomiya and Shibagaki, 2007; Xu *et al.*, 2009), thereby enhancing their capacity for causing catastrophic flooding (Doswell *et al.*, 1996).

In the summer of 2016, a particularly heavy rainfall event hit the YRB-ML during the period between 0000 UTC 30th June (hereafter 0630T00Z) to 0600 UTC 6th July (0706T06Z; see Figure 1a), with a record-breaking rainfall amount of 582.5 mm in Wuhan (30.60°N, 114.30°E; the provincial capital city of Hubei province) and several rain-gauge stations along the YRB-ML measuring rainfall rates in excess of 50 mm per hour. As a result, Wuhan suffered a terrific flooding disaster which inundated many roads, trapping residents inside vehicles and buildings. Overall, the event left about 237 dead and 93 missing, affected more than 10 provinces (Hubei, Anhui, Jiangsu, Jiangxi, Hunan, Chongqing and other provinces) and resulted in over \$22 billion in damage (Zhou *et al.*, 2018), making it a high-impact weather event of international significance.

Many studies have demonstrated the benefits of using convection-permitting models (CPMs) to predict severe weather (Bernardet *et al.*, 2000; Schwartz *et al.*, 2009; Weusthoff *et al.*, 2010), and convection-permitting ensemble systems have proved useful for simulating severe weather over the continental United States (Clark *et al.*, 2009; Xue *et al.*, 2013; Iyer *et al.*, 2016). Simulations with grid spacings of 1–5 km have begun to be used to investigate heavy rainfall over the Mei-yu region, but usually over relatively small domains (e.g., the lower reaches of the YRB), or focusing on a relatively short period of less than 1 day (Wang *et al.*, 2000; Liu *et al.*, 2008; 2010; Sun *et al.*, 2010; Luo *et al.*, 2014; Luo and Chen, 2015).

Although CPMs have numerous advantages for regional-climate simulation and weather prediction (Prein *et al.*, 2015), they also have limited domains in both space and time, and large computational costs, and can therefore usefully be complemented by simulations with global circulation models (GCMs) in numerical weather prediction (NWP) mode. For example, the development of climate models is often facilitated by using GCMs to conduct short-range (e.g., 5 day) predictions and adopting a process-oriented approach that employs observations for evaluating parameterizations (the so-called Transpose Atmospheric Model

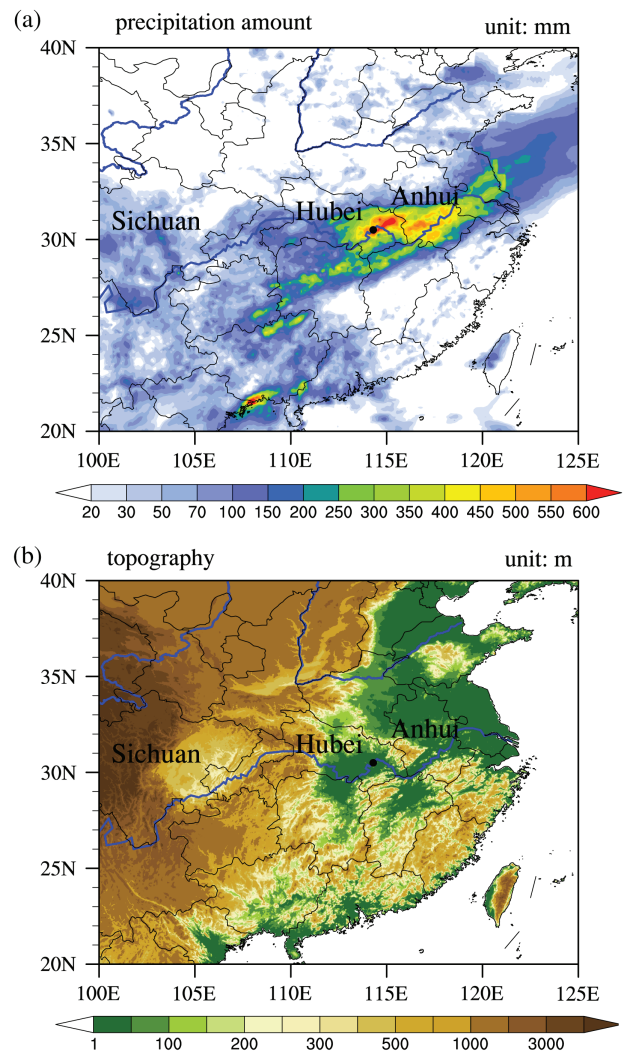


FIGURE 1 (a) Accumulated rainfall amount (unit: mm) from 0000 UTC 30th June (hereafter 0630T00Z) to 0600 UTC 6th July (hereafter 0706T06Z), 2016. (b) Topography distribution (unit: m) over eastern China. Here the text “Sichuan”, “Hubei” and “Anhui” indicates the location of Sichuan, Hubei and Anhui province, respectively. The black dot in (a) and (b) indicates Wuhan city, the provincial capital of Hubei province

Intercomparison Project (T-AMIP) methodology (Phillips *et al.*, 2004; Williams *et al.*, 2013). The use of short-range predictions minimizes the nonlinear interaction of systematic bias and allows the simulations to be validated against detailed observations (Williamson *et al.*, 2005; Klein *et al.*, 2006; Williamson and Olson, 2007; Boyle *et al.*, 2008). In this context, heavy rainfall events may be particularly useful objects of study, because they challenge the upper limits of global models. In particular, combining short-range predictions for cases of extreme flooding, with convection-permitting modeling and high-resolution observations, may help to pin down the key processes leading to model bias and investigate the added values of CPMs. Li *et al.* (2018) investigated the performance of the Climate System Model of Chinese Academy of Meteorological Sciences

(CAM5-CSM) in reproducing the spatial and temporal distribution of 2016 eastern China flooding. They found that the climate model has the ability to simulate the severity of the heavy precipitation event and the eastward movement of the southwest vortex, but the model struggled to reproduce the observed frequency-intensity structure and tended to produce an artificially steady center of heavy rainfall over a mountainous region. How well a higher-resolution model (e.g., a CPM) can simulate this heavy rainfall event remains unknown. In particular the extent to which a CPM prediction can “add value”, compared with lower resolution global climate model, has not been investigated before. This topic is of broader interest for two reasons: firstly, the adoption of high-resolution regional models for weather prediction has often been motivated partly by demonstrable improvements for simulations of specific heavy precipitation events (Clark *et al.*, 2009; Schwartz *et al.*, 2009; Weusthoff *et al.*, 2010; Kendon *et al.*, 2012; Xue *et al.*, 2013; Iyer *et al.*, 2016); secondly, understanding of the value and limitations of convection-permitting models for individual cases can be used to identify aspects of regional climate for which higher resolutions may be needed to obtain useful climate projections (Kendon *et al.*, 2017).

This work will use the 2016 eastern China flooding to identify aspects of model performance which are improved at convection-permitting resolutions, discriminate these from aspects which are not improved, and discuss the possible causes of the model's deficiencies. The remainder of the paper is organized as follows. Section 2 describes the models used, the experimental design, the observational datasets and reanalysis used to evaluate the simulations, and the analysis methods. Section 3.1 presents the observational features for this heavy rainfall event. Section 3.2 analyzes the results of two limited area simulations (LAMs) from the Met Office Unified Model (UM) and compares their results to the global driving model. Finally, in Section 4, we present a brief summary and draw some conclusions.

2 | METHODOLOGY

2.1 | Model and experimental design

A summary of experiments performed in this study is listed in Table 1. The experiments simulated by the Met

Office are from the Global NWP version of the Unified Model (UM), which are a rerun of operational forecast to study this heavy rainfall case. The UM atmosphere/JULES land surface configurations operational at this time were GA6.1/GL6.1 (Walters *et al.*, 2016) run at 25 km horizontal resolution and 70 levels in the vertical with model top at 80 km. The UM's ENDGame (Even Newer Dynamics for General atmospheric modelling of the environment) dynamical core uses a semi-implicit semi-Lagrangian formulation to solve the non-hydrostatic, fully-compressible deep-atmosphere equations of motion (Wood *et al.*, 2013). ENDGame, introduced with the GA5 configuration, is an evolution of the new dynamics incorporating a nested iterative timestep designed to improve accuracy, stability and scalability, and which significantly increases mid-latitude and tropical variability due to the reduction of implicit damping in the semi-Lagrangian advection. The model's physical parameterizations are described in detail in Walters *et al.* (2016) and the model relies on a mass-flux-based parameterization of convective clouds (Gregory and Rowntree, 1990) to produce most of convective rainfall (although the cloud microphysics will also produce some rainfall in convectively unstable columns). Apart from a very small number of differences the physics are consistent with the formulations (GA6/GL6) used in coupled model systems for seasonal, decadal and climate predictions/projections representing a seamless model prediction system.

For limited area modeling, we conduct LAMs with UM simulations (Walters *et al.*, 2016) at convection-permitting scales. The integration domain covers eastern China (20.3°N~42.0°N, 96.2°E~127.4°E). We use two sets of convection-permitting models, one with 0.02° (approximately 2.2 km) grid spacing (UM-2p2), the other is with 0.04° (4.4 km) grid spacing (UM-4p4). In the vertical direction, the model uses a terrain-following coordinate system composed of 80 vertical levels with lowest and highest model levels at 5 m and 38.5 km above the surface respectively. The resolutions of these configurations are sufficiently high for the non-hydrostatic dynamical core of the model to partially resolve sub-mesoscale convective motions, thereby negating the need for a convection parameterization (Lean *et al.*, 2008). Holloway *et al.* (2013; 2015) used the UM to investigate the effects of explicit versus parameterized convection on the

TABLE 1 A summary of experiments used in this study, including two convection-permitting limited-area simulations (LAMs; i.e., UM-4p4 and UM-2p2) and one global-driving model simulation (T-AMIP; i.e., UM-GL)

	Simulation	Horizontal resolution	Cumulus convection scheme based on
Convection-permitting simulation	UM-4p4	4.4 km	-
	UM-2p2	2.2 km	-
Global simulation	UM-GL	25 km	Gregory and Rowntree (1990)

Madden–Julian oscillation (MJO), they found that explicit convection simulations produce a stronger and more realistic MJO signal, as well as the associated vertical heating profile, compared with the simulations using convection scheme. On a subgrid-scale, additional vertical transport is provided by the non-local boundary-layer scheme of Lock *et al.* (2000) with some modifications (Boutle *et al.*, 2014) to make the scheme more applicable to the convective “grey-zone”. Liquid cloud masses and volume fractions are calculated in each grid box using a diagnostic cloud scheme based on a triangular probability density function for subgrid-scale relative humidity fluctuations (Smith, 1990). Subsequent microphysical processing the cloud, including nucleation and evolution of ice-phase particles, is governed by a four-species (cloud, rain, snow and graupel), single-moment scheme developed by Wilson and Ballard (1999), with subsequent extensive modifications by, e.g., Boutle *et al.* (2014), Furtado *et al.* (2015), and Wilkinson (2017). Both two LAMs are initialized at 0630T00Z by downscaling the Met Office operational global analysis. Boundary conditions for the LAMs are updated every hour from a global simulation performed with the UM at a resolution of 25 km. The duration of the simulations is 6 days, to encompass the period of intense Mei-yu activity within which the 2016 eastern China heavy rainfall event occurred.

All the numerical experiments performed in this study adhere to the T-AMIP standard. The T-AMIP integrations follow the experimental design described by Williams *et al.* (2013). All the three numerical experiments, including one global and two limited area simulations, were produced for the period from June 29th to July 5th, 2016. The simulations were initialized at 1200 UTC at each day and integrated for 6 days. The first 12 hr of each simulation was discarded as a spin-up and we use 13–36 hr of each simulation for analysis in this study. To enhance the comparability between observation and model simulation, the outputs from the simulations were interpolated onto the same grid as the observations or reanalysis.

2.2 | Observation and reanalysis dataset

In this study, we use a merged rain gauge-satellite gridded hourly precipitation dataset for China (Pan *et al.*, 2012; Shen *et al.*, 2014), developed by the China Meteorological Administration (CMA). This product uses the probability density function optimal interpolation (PDF-OI) technique to combine hourly surface rainfall measurements from CMA's network of rain gauges with a satellite-retrieved precipitation product based on the Climate Prediction Center's morphing technique (CMORPH; Joyce *et al.*, 2004). The regional merged product has a spatial resolution of approximately 10 km and has been shown to greatly reduce regional biases, particularly for heavy-rainfall, compared with the former

version (Shen *et al.*, 2014). The dataset contains significantly more stations than those used in previous studies (Yu *et al.*, 2007a; 2007b; Zhou *et al.*, 2008; Pan *et al.*, 2012; Shen *et al.*, 2014) and has been used to study the precipitation statistics of southern China (Luo *et al.*, 2013; Jiang *et al.*, 2017).

We use the 6-hr surface pressure, vertical velocity (ω), zonal (u) and meridional (v) components of the wind, specific humidity (q), geopotential height (GPH) and temperature (t) variables derived from ERAIM reanalysis dataset (Dee *et al.*, 2011) to reveal the large-scale circulations associated with the Wuhan heavy rainfall event. The spatial resolution of ERAIM is 0.125° (about 12.5 km). We also use the hourly high-resolution realization (HRES; about 31 km) ω , u , v , t , q and GPH derived from ERA5 reanalysis dataset to reveal the hourly evolution of dynamical features associated with Wuhan heavy rainfall event, which was developed through the Copernicus Climate Change Service (C3S). ERA5 is the fifth generation of the ECMWF atmospheric reanalysis of the global climate (<http://climate.copernicus.eu/products/climate-reanalysis>). In addition, we also use the topography derived from Global 30 Arc-Second Elevation (GTOPO30, available from the U.S. Geological Survey) to review the spatial distribution of terrain over eastern China.

2.3 | Analysis method

In this study, the precipitation frequency (PF) is defined as the percentage of all hours during the studying period (from 0630T00Z to 0705T23Z) which has measurable precipitation (≥ 0.1 mm/hr).

To verify the spatial distribution of rainfall in the simulations, the fractional skill score (FSS; Roberts and Lean, 2008) is used and more details can be found in their literature. The FSS shows how the skill of a simulation varies with different spatial scale and different precipitation threshold. The FSS has a value that varies between 0.0 and 1.0, and the higher FSS value means the model has better performance in reproducing the spatial distribution of precipitation. Generally speaking, the FSS increases with spatial scale (i.e., neighborhood size) until the desired level of skill has been reached (Roberts and Lean, 2008). In our analysis, the FSS was applied to a variety of different neighborhood sizes (30, 50, 70, 90, 110, 130, 150, and 170 km) with different precipitation thresholds depending on the three different time-slices we focused during the whole period of interest.

3 | RESULTS

In the following analysis, we firstly give an overview of the Wuhan heavy rainfall event, by describing the observed precipitation characteristics and the associated large-scale circulations. Subsequently, the performance of three model simulations (two LAM simulations and one global simulation),

in reproducing the spatial distribution of accumulated rainfall amount, daily precipitation and the evolution of rainfall belt, is investigated. We aim to find the added values of CPM in reproducing the spatial distribution of precipitation, precipitation structure, the diurnal cycle of precipitation and topographical rainfall, compared with global driving model (UM-GL). Finally, a brief summary is given in Section 4.

3.1 | Observed characteristics of 2016 eastern China heavy precipitation

The spatial distribution of the accumulated precipitation amount and the topography are shown in Figure 1. The heaviest rainfall was centered on the YRB-ML and covered a wide area which delineates the mean position of the monsoon front during the heavy-rainfall period (Figure 1a). The observations show that the accumulated rainfall amount, over most of the affected area, exceeded 400 mm during the raining period. In some parts of eastern Hubei province and southern Anhui province, the accumulated rainfall amount reached up to 600 mm. A record-breaking accumulated rainfall amount of 582.5 mm was measured at Wuhan-station. At Jiangxia (30.35°N, 114.32°E), a district in Wuhan, the accumulated rainfall amount was 733.5 mm. These large accumulations resulted from the persistent occurrence of exceptionally high rainfall rates, for example, hourly precipitation intensities in excess of 50 mm/hr were recorded at several rain gauge stations along the YRB-ML (figures not shown). These statistics are indicative of a long-duration and high precipitation intensity, which concentrated huge rainfall accumulations into a relative small region.

The occurrence of the heavy rainfall event was associated with the large scale synoptic circulations (Figure 2). The heavy rainfall was accompanied by the generation of an eastward moving low-level vortex that formed over Sichuan basin (around 30°N, 106°E) on 30th June (Figure 2a), and a relatively strong southwesterly low-level jet (LLJ) along the north-west flank of the western North Pacific subtropical high (WNPSH) in the lower troposphere (Figure 2a). On 1st July, the low-level vortex moved eastward from 106°E to 110°E and its intensity was enhanced (Figure 2b). The sites of heaviest rainfall in Hubei and Anhui provinces were located on the eastern side of the low-level vortex (Figure 2b). Meanwhile, the Mei-yu front began to form over the YRB-ML (to the east of the vortex center). In Figure 2b–e, the front is visible as a region of large meridional gradients of equivalent potential temperature (θ_e) and a distinct sharp horizontal wind shear line. The strong LLJ brought high θ_e (above 345 K), i.e., warm and moist air, from lower latitudes into the Mei-yu frontal zone. To its north, cold-dry (low θ_e) air, from higher latitudes, converged with warm-moist air over Mei-yu frontal zone (Figure 2b). The combination of sustained moisture supply and the merging of distinct air masses along the frontal zone

was highly conducive to the formation and development of the mesoscale convective systems in the Mei-yu front. Eventually the Mei-yu front exhibited a southwest-to-northeast spatial distribution and lasted for another 3 days (Figure 2c–e), and began to disappear on 5th July (Figure 2f).

3.2 | Met Office unified model simulations

3.2.1 | The evolution of heavy precipitation

A comparison of evolution in time of the meridional-averaged rainfall, between observations and simulations, is shown by the time-versus-longitude (Hovmöller) plots in Figure 3. The whole studying period (encompassing 6 days) can be separated as two periods due to different large-scale circulations: a period of eastward propagation from 0630T00Z to 0701T23Z (the first time period, hereafter P1; Figure 3a), mainly affect by an eastward moving low-level vortex; a second time period (P2, from 0702T00Z to 0705T23Z; Figure 3a), when the Mei-yu front formed over YRB-ML and the large-scale circulations became more “quasi-stationary”. During the second period, successive heavy rainfall systems can be seen propagating eastward along the quasi-stationary front.

In the observations, the rainfall system underwent an obvious, large-scale eastward propagation (from 104.0°E to 124.0°E) during P1 (Figure 3a). During this transition, the system leaved a narrow rain band (about 250 km in width), oriented from west-to-east over the YRB-ML and the maximum accumulated rainfall amount reached up to 350.0 mm (Figure 4a). All three models capture this overall large-scale eastward “jump” in the position of the rainfall, and UM-4p4 (Figure 3c) and UM-2p2 (Figure 3d) show better skill in reproducing the eastward propagation of smaller-scale disturbances within the propagating system during the first 36 hr (from 0630T00Z to 0701T12Z). UM-4p4 and UM-2p2 are also better at reproducing the east–west axis of the rain band along the YRB-ML and the heavy rainfall center where the accumulated rainfall exceeds 150.0 mm (Figure 4e,g). We now quantify all the model performance in reproducing the spatial distribution of precipitation by using FSS values and show some results for the accumulations during P1 to increase the signal for the higher thresholds (Figure 5). The typical behavior of the FSS values is that they increase with larger horizontal scales (Figure 5a,d,g). It is evident from the Figure 5f that at higher rainfall totals (higher than 150.0 mm), CPM has larger FSS values compared to global driving model, signifying that CPM could better reproduce the spatial distribution of higher rainfall amounts. However, both high-resolution configurations frequently produce excessive rainfall rates during P1 (Figure 3c,d).

Although UM-GL could also partly reproduce the eastward “jump” during P1, it struggles to produce coherent west-to-east propagating small-scale features within the rain-belt (Figure 3b). For example, it has less rainfall around

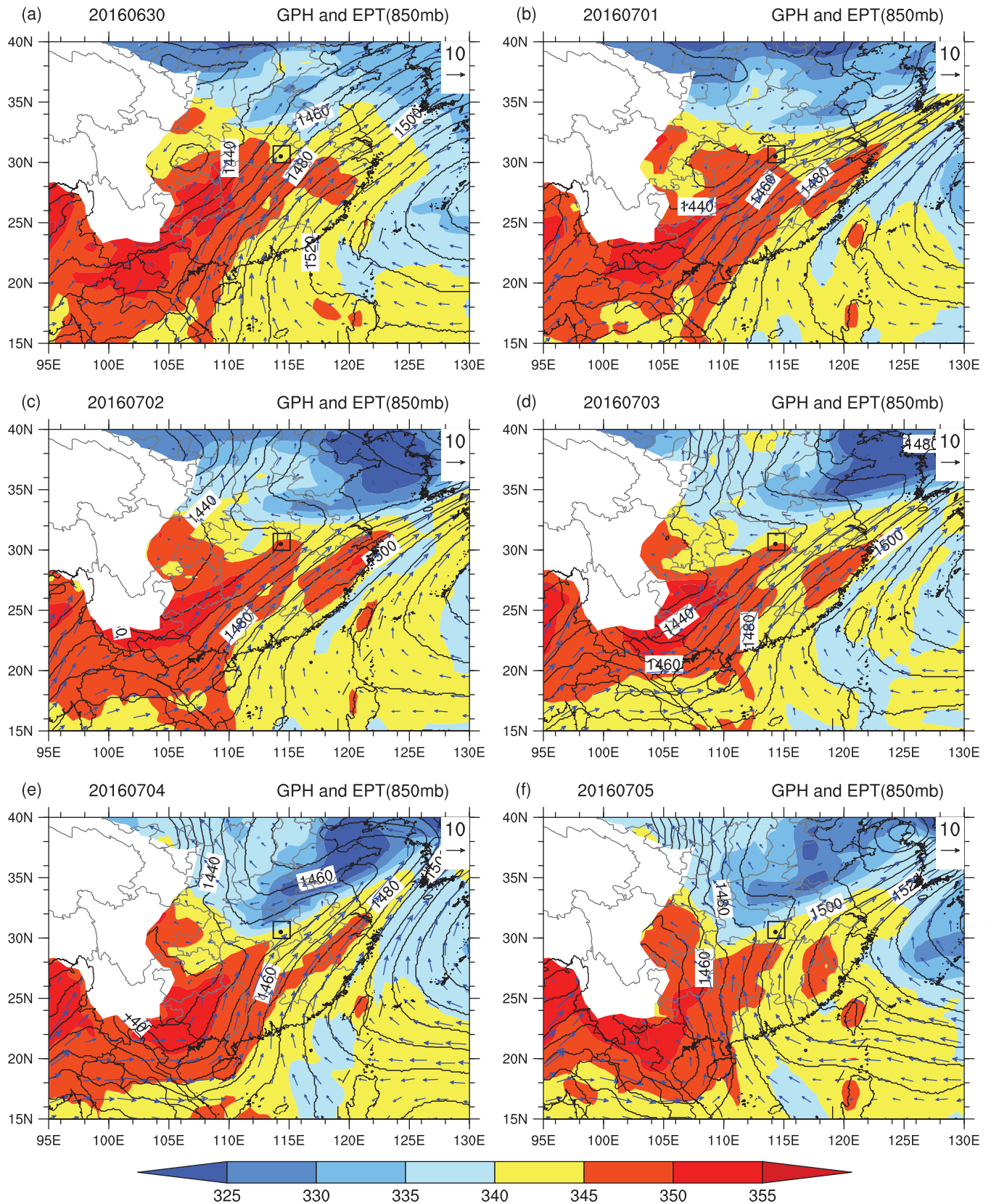


FIGURE 2 The synoptic large-scale circulation during studying period: the equivalent potential temperature (θ_e ; shaded, unit: K), GPH (contour, unit: gpm) and wind vectors (vector, unit: m/s) at 850 hPa on (a) 30th June, (b) 1st July, (c) 2nd July, (d) 3rd July, (e) 4th July and (f) 5th July. The area higher than 1,500 m is masked out. The black dot and rectangle indicate Wuhan city and its surrounding region

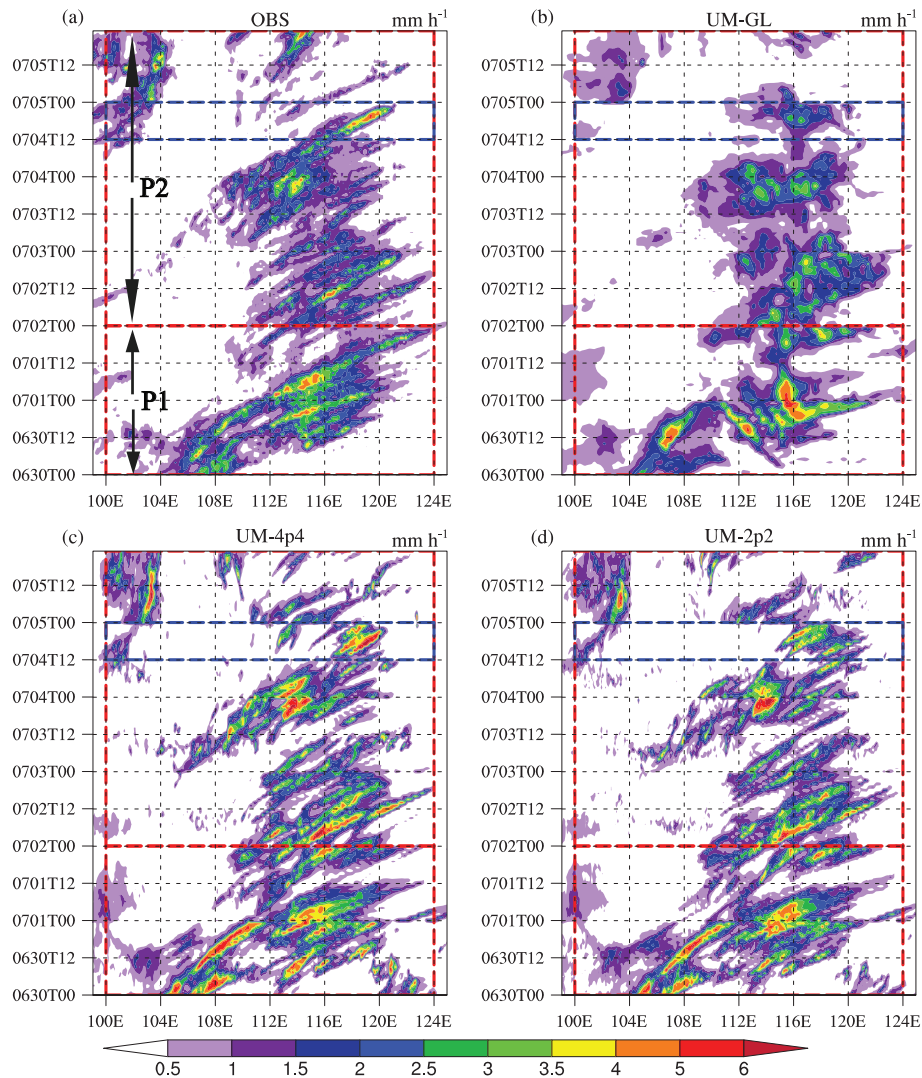


FIGURE 3 The evolution of rainfall (time versus longitude) averaged between 27°N and 33°N (unit: mm/hr) in observation and simulation: (a) observation, (b) UM-GL, (c) UM-4p4, (d) UM-2p2. Here two red dashed rectangles in (a) indicate two time period: P1 is the first time period from 0630T00Z to 0701T23Z, P2 is the second time period from 0702T00Z to 0705T23Z. The blue dashed rectangle denotes a short time period of P2 from 0704T12Z to 0705T00Z

108.0°E~110.0°E in eastern Sichuan basin, and on 1st July the simulated rainfall occurs preferentially over a mountainous region (around 30.5°N, 116.0°E) which is more stationary than was observed (Figure 3b), and also produces a spurious westward moving system (from 115.0°E to 110.0°E; Figure 3b). As a result, the spatial distribution of rainfall in UM-GL is not as good as in UM-LAMs during P1 (Figure 5f).

During P2, the Mei-yu front formed and the synoptic situation was more stationary than during P1 (Figure 2c–f). Successive heavy rainfall systems travel along the YRB-ML in observations (Figure 3a). The rain-belt had a southwest-to-northeast axis and the heaviest rainfall is located in southern Anhui Province (Figure 4b). UM-GL tends to generate steady heavy rainfall over mountainous region (Figure 3b) and cannot reproduce heavy rainfall systems propagating eastward along the Mei-yu front (Figure 3a). In comparison to UM-GL, both UM-LAMs show better

performance in reproducing the eastward-propagation process during P2 (Figure 3c,d) and show closer resemblance to the observations in this aspect of the spatial distribution (Figure 4f,h). For example, the UM-LAMs are better at simulating a train of heavy rainfall systems which travel from 117°E and 120°E between 0704T12Z and 0705T00Z (Figure 3c,d), and they are better at reproducing the heavy rainfall center (above 20.0 mm) in both its intensity and location (Figure 5i). More details of this time period will be further investigated in the later section.

3.2.2 | The eastward propagation of rainfall system during P1

During P1, the evolution of the heavy precipitation was highly correlated with the eastward-propagating low-level vortex (LLV; Figure 6). The strong LLV could enhance the gradient

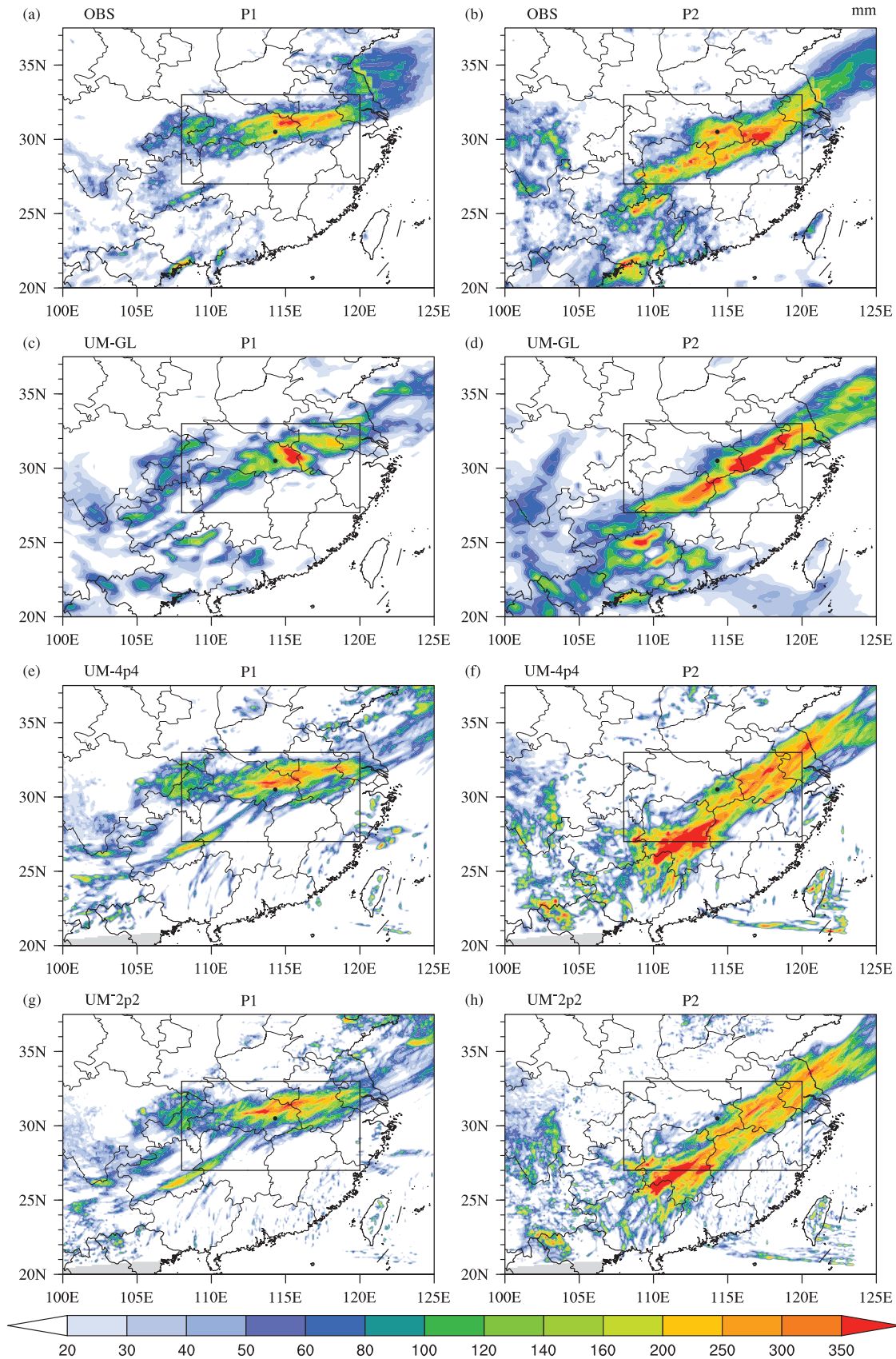


FIGURE 4 Observed and simulated precipitation amount (unit: mm) during two time periods, (a), (c), (e), (g) are the first period (P1); (b), (d), (f), (h) are the second time period (P2) among: (a), (b) observation, (c), (d) UM-GL simulation, (e), (f) UM-4p4 simulation, (g), (h) UM-2p2 simulation. The rectangle indicates the main rainfall center (i.e., the control region; $108^{\circ}\text{E}\sim 120^{\circ}\text{E}$, $27^{\circ}\text{N}\sim 33^{\circ}\text{N}$) to perform the investigation of some detailed precipitation characteristics. The black dot indicates Wuhan city

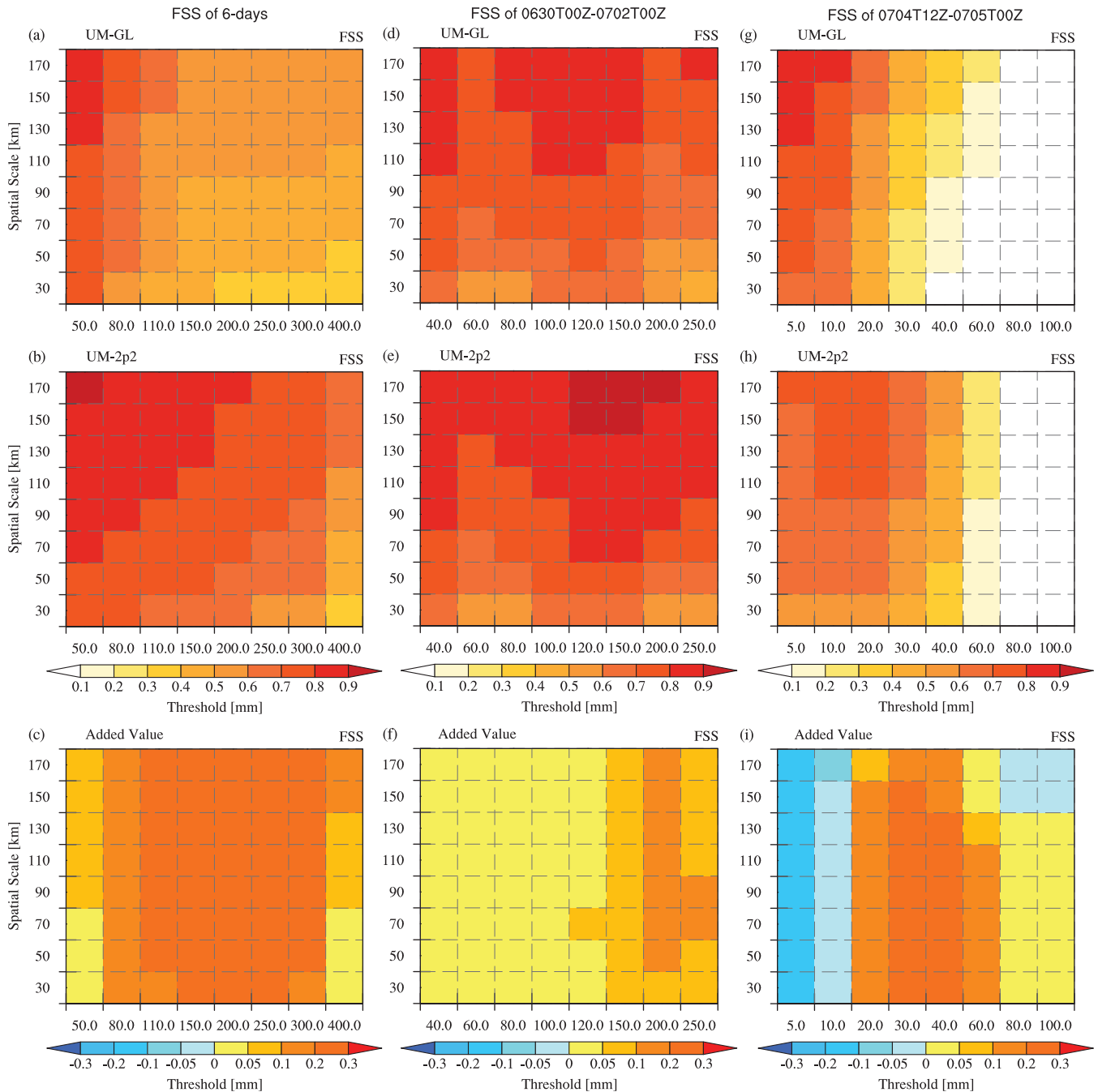


FIGURE 5 Fractional skill score (FSS) during the time period of (a), (b), (c) 6-days from 30th June to 5th July; (d), (e), (f) P1 time period from 0630T00Z to 0701T23Z; (g), (h), (i) a short time period of P2 from 0704T12Z to 0705T00Z; (a), (d), (g) are the FSS of UM-GL; (b), (e), (h) are the FSS of UM-2p2; (c), (f), (i) are the added value of UM-2p2 (the added value is defined as the FSS of UM-2p2 minus the FSS of UM-GL)

of GPH between southeast and northwest area, and also induced an associated cyclonic circulation, both were favorable for accelerating the low-level jet (LLJ) over southeastern China (Figure 6). The heavy rainfall center preferred to trigger and develop to the east of the LLV and moved with the LLV (Figure 6a–m). Meanwhile, the LLJ was enhanced during the development of LLV, and reached its maximum at 0630T21Z (Figure 6h). The strong LLJ brought abundant moisture and induced intense upward motion over middle to the YRB-ML, thus caused heavy rainfall and induced the

first rainfall peak over the main rainfall center (i.e., the control region; 108°E~120°E, 27°N~33°N). The intensity of the LLV weakened gradually after 0701T12Z (Figure 6m–p), but the GPH over eastern part of Sichuan basin could remain its strength and thus dominated the daily mean LLV center (which was located on the west of Wuhan city in Figure 2b).

The tracks of the LLV in ERA5 and model simulations are shown in Figure 7. The LLV was generated and enhanced in the Sichuan valley on 30th June, and moved eastward along the YRB-ML on 30th June and 1st July (Figure 7a). All three

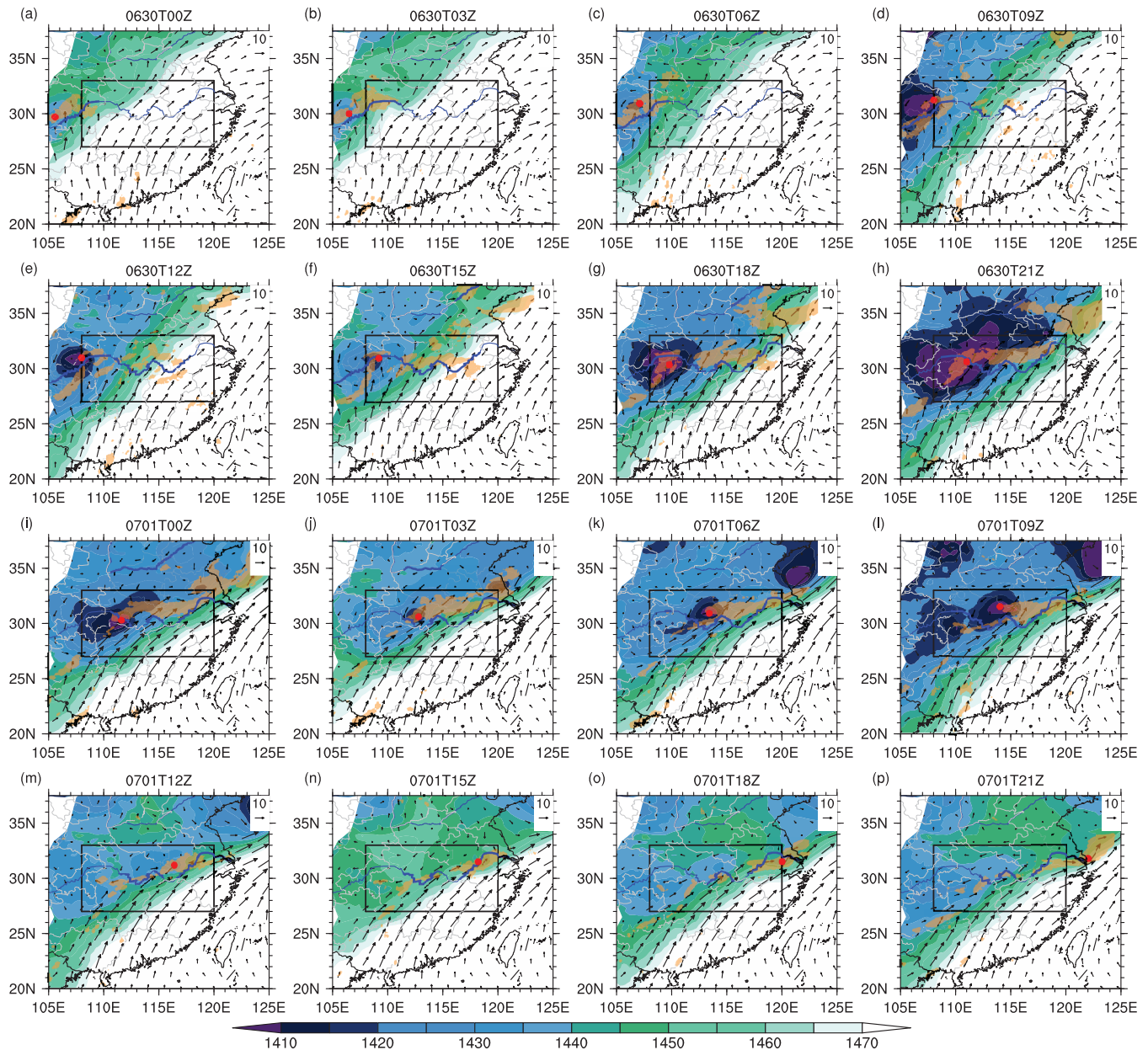


FIGURE 6 3-hr evolution of low-level vortex (shading indicates the GPH; unit: gpm), horizontal wind fields (vector; unit: m/s) at 850 hPa in ERA5, and 3-hr accumulated precipitation (around each specific time; the orange shading indicates the region where the accumulated rainfall over 10.0 mm) in observation during P1. Here the red dot indicates the center of eastward propagating low-level vortex (location of minimum GPH)

models could reproduce the eastward movement of LLV on the first 36 hr (from 0630T00Z to 0701T12Z), although the eastward propagation of LLV in model simulations is slower than in ERA5 (Figure 7b–d). All three models fail to reproduce the eastward movement of LLV in the last 12 hr during P1 (from 0701T12Z to 0702T00Z; Figure 7b–d). During this time period, the LLV in ERA5 began to vanish but still moved eastward after 0701T12Z, it was located at around 120.0°E in the lower reaches of YRB (Figure 7a); Meanwhile, the low GPH on the west of Wuhan city (around 114.0°E), linking with the low pressure system over eastern Sichuan basin, could remain its strength (Figure 6m–p). CPMs and UM-GL could reproduce the western branch of the LLV which was still

located on the west of Wuhan, but they all struggled to simulate the eastward-propagating LLV and the associated rainfall. Therefore, all three models fail to reproduce the spatial distribution of precipitation to the east of 120.0°E during the last 12 hr of P1 (Figure 3b–d), especially over coastal and ocean region (Figure 4c,e,g).

To validate the performance of the models in reproducing the dynamical features of LLV, the time series of minimum GPH at the center of LLV and the GPH averaged over the control region are shown in Figure 7e,f. As mentioned above, the LLV was formed and enhanced over Sichuan valley, it reached its maximum intensity at 0630T21Z, when the GPH at the core of LLV is 1,386.5gpm in ERA5 (black line in

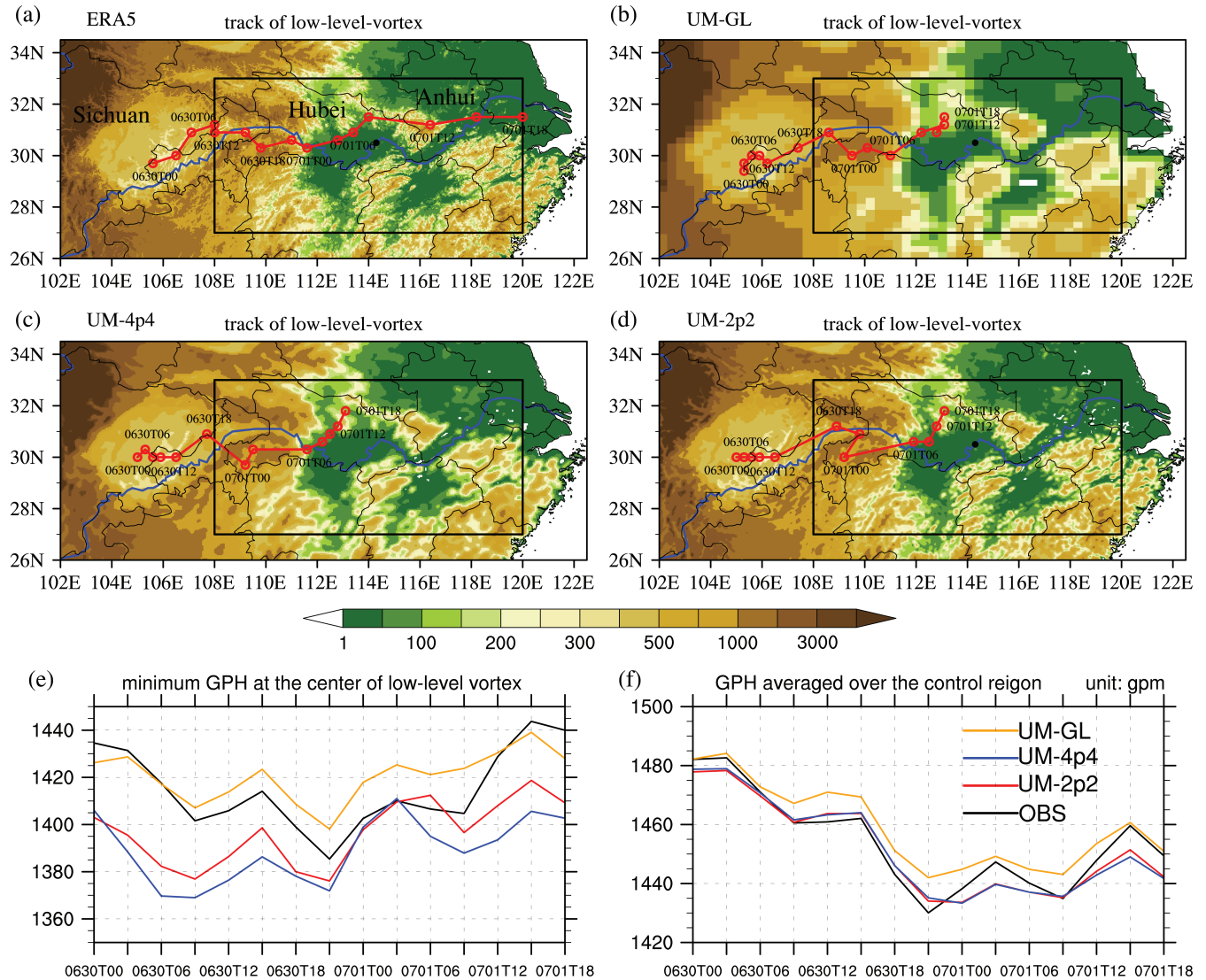


FIGURE 7 The track of low level (850 hPa) vortex (defined as the location of minimum geopotential height of the low-level vortex; red line) in (a) ERA5 reanalysis, (b) UM-GL, (c) UM-4p4 and (d) UM-2p2 simulation. The location of the low-level vortex is indicated by red hollow at 3-hr intervals and labeled by 6-hr time intervals. The shading indicates the topography derived from GTOPO-2MIN and used in each model simulation. The Yangtze River and Yellow River in (a)-(d) are denoted as blue lines. The black rectangle indicates the control region. (e) Time series of minimum geopotential height (GPH) at the center of low-level vortex; (f) time series of GPH averaged over the control region. Here the black line indicates the observation, the red line for UM-2p2, the blue one for UM-4p4 and the orange line for UM-GL

Figure 7e). After this, the LLV continued to move eastward and its intensity decreased. All three models could reasonably reproduce the evolution of LLV intensity (Figure 7e). But both LAMs (red and blue lines) overestimated the intensity of the eastward-propagating LLV, linking with excessive simulated precipitation in models, similar phenomena could also be found in other studies (Zhang *et al.*, 1988; Molinari and Dudek, 1992; Zhang *et al.*, 1994), while UM-GL (orange line) underestimated the intensity at the center of LLV (Figure 7e). CPMs are better at reproducing the evolution in time of GPH averaged over control region (red and blue lines in Figure 7f), UM-GL underestimated the averaged GPH intensity over the control region (orange line).

3.2.3 | The added value and weaknesses of UM-LAMs at convection-permitting scales

The above analysis suggested that CPMs can have added value compared with the lower-resolution simulations in terms of the amount and spatial distribution of precipitation, particularly where this is related to small-scale features within the rain-belt. In this section, we will study this in more detail by investigating the differences between CPMs and their global driving model in terms of their precipitation “intensity-frequency” structures, diurnal cycles and topographic rainfall. Firstly, in Figure 8, we investigate whether CPMs could better simulate the time series of hourly precipitation rates (mm/hr) averaged over the main rainfall center

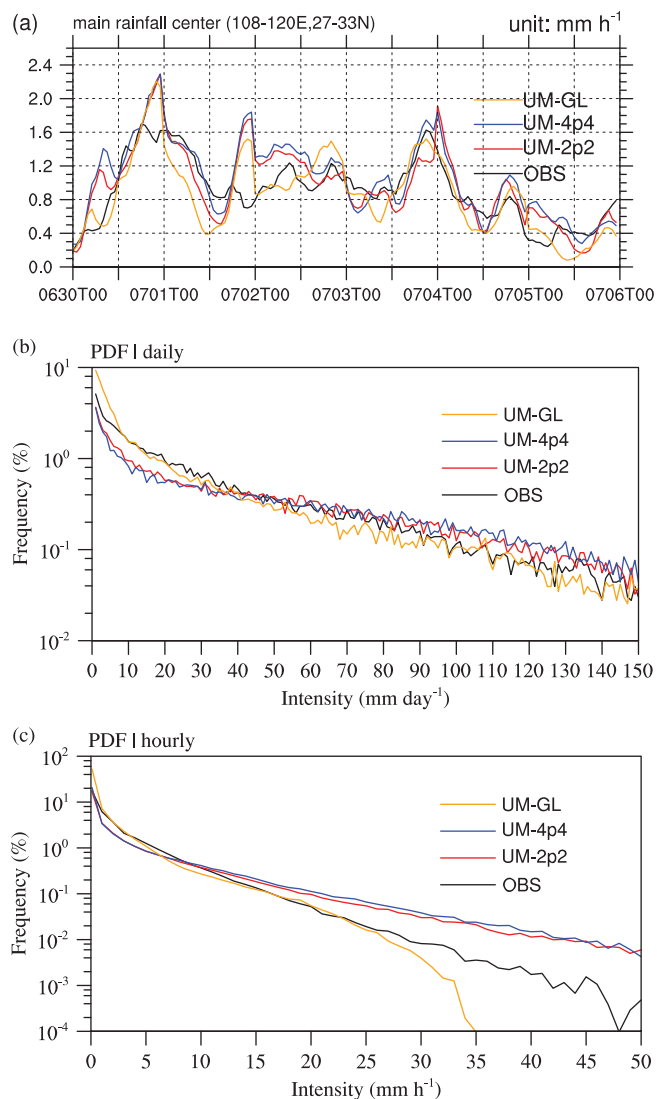


FIGURE 8 (a) Time series of precipitation rates (unit: mm/hr) and (b) probability distribution function (PDF) of daily precipitation over the control region (108°E~120°E, 27°N~33°N), during the time period 0630T00Z to 0705T23Z, (c) the same as (b), but for hourly precipitation. Here the black line indicates the observation, the red line for UM-2p2, the blue one for UM-4p4 and the orange line for UM-GL

(108°N~120°E, 27°N~33°N). In the observations, there are two major peaks of precipitation over the YRB-ML. The first peak is around 0701T00Z and the second peak is around 0704T00Z (Figure 8a). All three models successfully simulate the evolution of hourly precipitation averaged over the main rainfall center and reproduce the two major precipitation peaks, but overestimate the magnitude of the first peak (Figure 8a). All three simulations have too much precipitation from 0701T18Z to 0702T00Z during P1 (Figure 8a). Hence, we conclude that there is little advantage of CPMs over the global model in terms of the regionally averaged precipitation for this heavy rainfall event.

It has been noted in previous studies (e.g., Clark *et al.*, 2009; Weusthoff *et al.*, 2010; Xue *et al.*, 2013; Kendon

et al., 2017), that CPMs are sometimes better able to reproduce heavy rainfall, compared to convection-parameterized models. To investigate the realism of the heavy rainfall predicted for this case, Figure 8b,c show the frequency-intensity distributions of precipitation on daily- and hourly-time scales. On a daily time scale, UM-GL (Figure 8b; orange line) severely overestimates the light precipitation (less than 10 mm/day) and underestimates the rainfall at the range from 40.0 to 90.0 mm/day (Figure 8b). This over/under-estimation of light/heavy rain is a long-standing problem for convection-parameterized models, including both GCMs and RCMs (Dai *et al.*, 1999; Ban *et al.*, 2014; Fosser *et al.*, 2015). By contrast, UM-4p4 (blue line) and UM-2p2 (red line) have a relatively good performance in simulating the rainfall ranging from 40.0 to 90.0 mm/day, but they both underestimate the frequency of drizzle, and produce more very-heavy precipitation (greater than 90.0 mm/day) than was observed (Figure 8b), which are consistent with the findings of previous studies (e.g., Kendon *et al.*, 2012; Fosser *et al.*, 2015). Those phenomena are also evident at hourly scale: UM-GL produces too much light rainfall below 2.0 mm/hr and does not simulate enough precipitation above 25.0 mm/hr (Figure 8c); UM-4p4 and UM-2p2 underestimate the rainfall in the range of 2.0 to 8.0 mm/hr, and frequently produce excessive rainfall rates (above 10.0 mm/hr; Figure 8c).

The diurnal variations in precipitation are also an important aspect of this kind of severe weather and moreover have been a rigorous test-bed for evaluating numerical model performances in general (Chen *et al.*, 2017; Li *et al.*, 2018). The 6-day composite diurnal cycle of precipitation and spatial distribution of the Beijing standard time (BJT) of maximum precipitation are shown in Figure 9. In the observations, the results show that the diurnal variation of precipitation within the monsoonal rainfall belt is dominated by the early-morning rainfall (around 0400 BJT; Figure 9b); the diurnal cycle of precipitation over areas outside of the major rainfall belt (for example, southeastern China) are controlled by the afternoon rainfall (from 1400 BJT to 1800 BJT; Figure 9b). All three models could successfully reproduce the early-morning rainfall within the major rainfall belt (Figure 9c–e). The simulated rainfall shows an early morning rainfall peak (0500 BJT) that is more pronounced than observed, and the afternoon precipitation is also excessively suppressed in UM-GL (Figure 9a), thus it overestimates the amplitude of the diurnal variations, compared to the observations and CPM simulations.

The longitudinal profiles of accumulated rainfall (unit: mm) and topography (unit: m) averaged between 29.5°N and 31.5°N over the whole studying period are shown in Figure 10a. The observed 6-day accumulated rainfall (black line) averaged over 29.5°N~31.5°N reached up to 400.0 mm between 114.0°E and 118.0°E (Figure 10a). In UM-GL (orange line) the precipitation is anchored over the relative higher terrain around 116.0°E, leading to severe

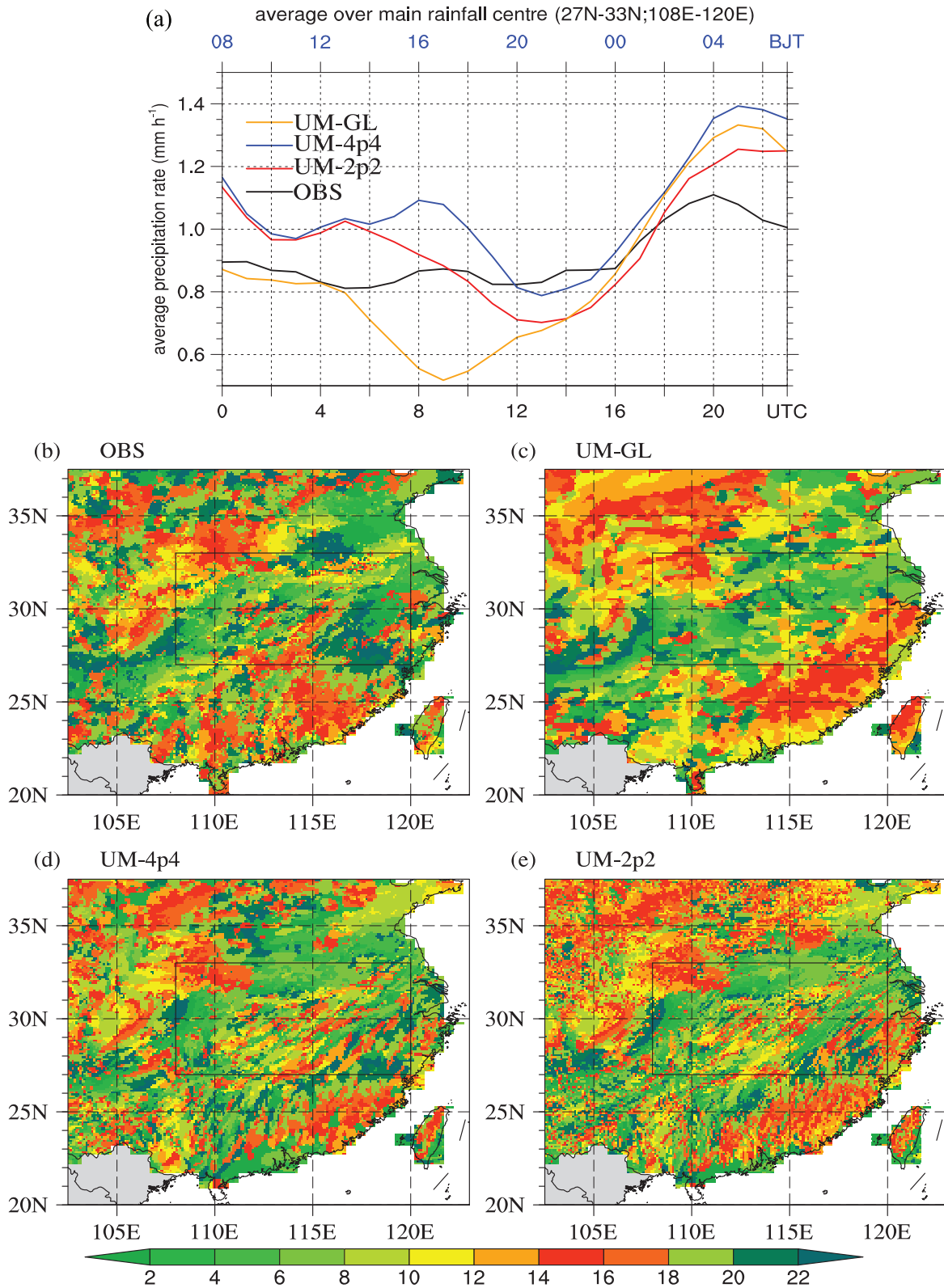


FIGURE 9 The 6-day composite diurnal cycle of precipitation and spatial distribution of Beijing standard time (BJT; the unit of the upper x-axis) of maximum precipitation. (a) The regional-averaged composite diurnal cycle of precipitation (mm/hr) over the control region (108°E~120°E, 27°N~33°N), during the studying period from 0630T00Z to 0705T23Z. Here the black line indicates the observation, the red line for UM-2p2, the blue one for UM-4p4 and the orange line for UM-GL. (b)-(e) are the spatial distribution of preferred time (BJT) of maximum precipitation: (b) observation; (c) UM-GL; (d) UM-4p4; (e) UM-2p2

overestimation of rainfall in this region. This implies that the effects of orographic-uplift are magnified in UM-GL. Similar model bias were also found in another global convection-parameterized CAMS-CSM (Li *et al.*, 2018), who attributed the source of the excessive orographic precipitation as being due to the inadequacies in the representation of the effect of the local topography. The simulated rainfall accumulations over mountainous region reach up to 600.0 mm, which is 1.5 times as much as observations. UM-4p4 (blue line) and UM-2p2 (red line) reduce the spurious topographical rainfall observed in the global model, and better simulate the precipitation in both spatial distribution and magnitude (Figure 10a). To further demonstrate the improvements in the model response to the topographic forcing, Figure 10b–e show the time-averaged precipitation frequency (PF) during the whole studying period. In the observations, the averaged PF over the control region is 35.2%, and has a maximum of 75.0% over the control region (Figure 10b). UM-GL overestimates the PF, with the simulated PF exceeding 95.0% over mountainous region (Figure 10c). This implies that precipitation is almost always occurring over the small mountain in UM-GL. By contrast, UM-4p4 (Figure 10d) and UM-2p2 (Figure 10e) show closer resemblance to the observations, although the PF are slightly underestimated in UM-LAMs.

To further examine the model behavior in simulating the small-scale features of precipitation, a short period from 0704T12Z to 0705T00Z during P2 is investigated (Figure 11). The time series of precipitation averaged over mountainous region are shown in Figure 11a. It can be seen that UM-GL overestimates the precipitation over the small mountain during the period from 0704T12Z to 0705T00Z, producing five times more rainfall than was observed (Figure 11a). The spatial distribution of precipitation and the associated atmospheric circulations, during this time period, are shown in Figure 11b–e). In the observations, there is a narrow heavy rainfall center to the southeast of mountain, and the maximum accumulated rainfall amount during the 12-hr period exceeded 80.0 mm. This heavy rainfall center is associated with the mesoscale cyclonic circulation to the west of mountain, and there is relatively little precipitation over mountainous region itself (the blue box in Figure 11b). Both UM-4p4 and UM-2p2 successfully simulate the occurrence and position of the narrow heavy rainfall center (Figure 5i), although they overestimate the amount of rainfall (Figure 11d,e). They also give a better representation of the low-level flow in the vicinity of the mountain (Figure 11d,e). Although UM-GL better reproduces the light rainfall (under 10.0 mm; Figure 5i; Figure 11c) compare with CPMs, it cannot reproduce the low-level flow. Instead, UM-GL has too much convergence over the upwind slope of mountainous region (Figure 12a), more intense upward motion (Figure 12b) and more total column water vapor (Figure 12c), which has significant modulation of the wet precipitation bias over the inner key region,

and cannot simulate the heavy rainfall center in the right place (Figure 11c).

4 | SUMMARY AND DISCUSSION

4.1 | Summary

An extremely heavy rainfall event hit YRB-ML from June 30th to July 6th, in 2016. This event was characterized by high precipitation intensity, long duration rainfall and was associated with large-scale circulations that were favorable for producing extremes of organized deep convection in the Mei-yu front region. In particular, an eastward moving low-level vortex and westward development of the WNPSH enhanced atmospheric instability and increased the moisture supply, creating the conditions for producing a long-lived quasi-stationary convergence zone in the Mei-yu region. The strong south-westerly LLJ brought abundant warm and moist air from lower latitudes into the Mei-yu front, and cold air from higher latitudes penetrated the Mei-yu front, triggering intense upward motion and heavy rainfall due to convergence.

The whole studying period could be separated into a propagating phase (P1), followed by a quasi-stationary (Mei-yu) phase (P2), due to different large-scale circulations. During P1 (from 0630T00Z to 0701T23Z), the rainfall propagated eastward from 104.0°E to 124.0°E due to the motion of a LLV. UM-GL could partly reproduce the eastward “jump” of rainfall during P1, but it is unable to produce the coherent propagating small-scale features of rain-belt. It could not produce enough precipitation in the eastern Sichuan basin (108.0°E~110.0°E) and southern Anhui province (to the east of 116.0°E). By comparison, UM-4p4 and UM-2p2 have more skill in reproducing the eastward propagation of smaller-scale disturbances within the rain-belt during P1, and are better at simulating the resulting east-to-west-oriented rain band. In particular, they provide a better simulation of the location and intensity of the heavy rainfall center where the accumulated rainfall exceeded 150.0 mm. None of the three models produced enough precipitation to the east of 120.0°E in the last 12 hr during P1, because the LLV stalled in the middle YRB, instead of travelling further eastward as was observed.

The synoptic condition becomes more stable and individual heavy rainfall systems move from west to east along the Mei-yu front over YRB-ML during P2 (from 0702T00Z to 0705T23Z). UM-GL produces too much light rainfall, suppresses afternoon rainfall, and magnifies the uplifting effects of small mountains. Excessive convergence over mountainous terrain leads to steady heavy rainfall in the wrong parts of the domain. In comparison to UM-GL, UM-4p4 and UM-2p2 show better performance in reproducing the successive eastward-propagating heavy rainfall systems during P2, although they produce more heavy precipitation than

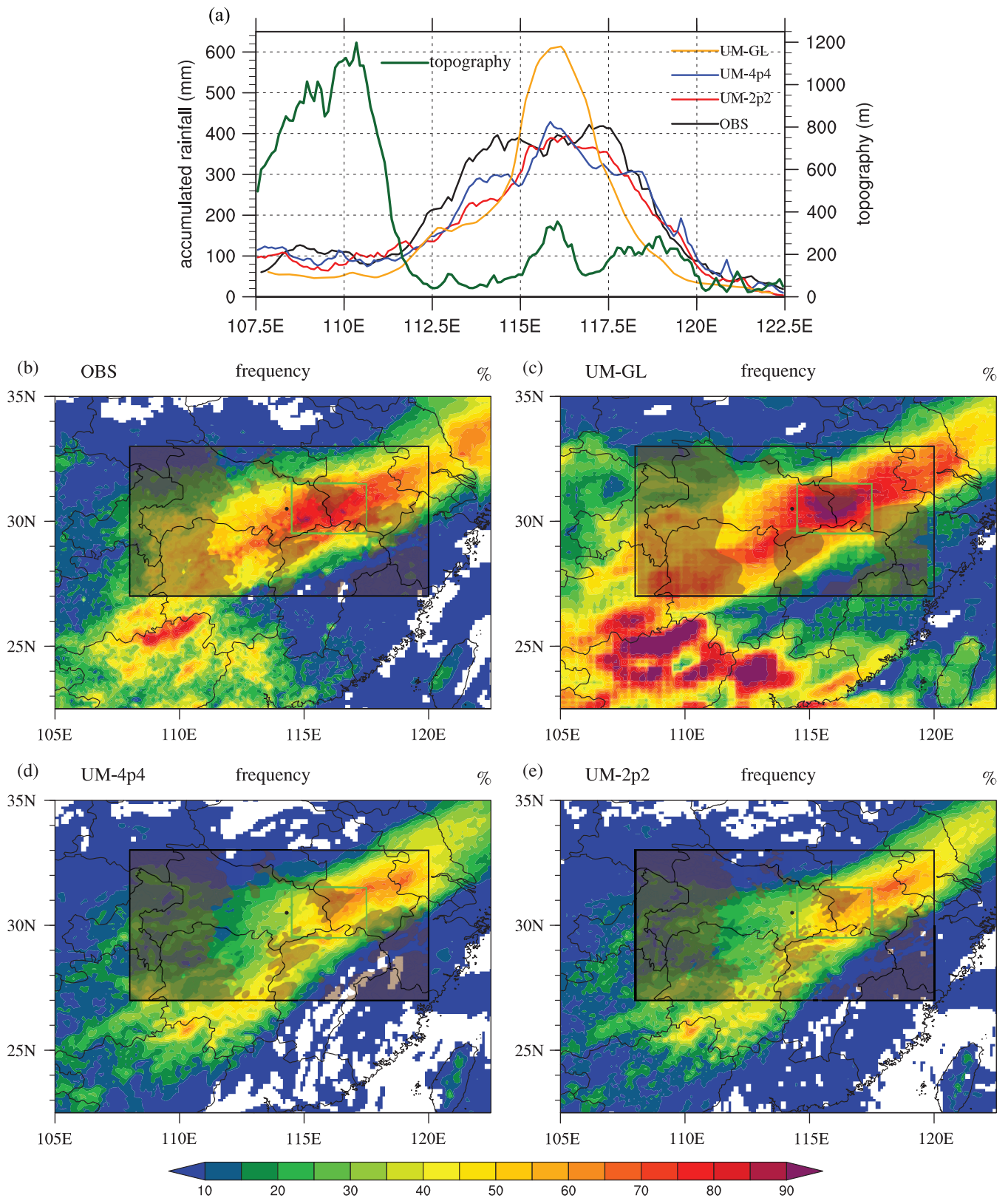


FIGURE 10 (a) The longitude profile of accumulated rainfall (unit: mm) and topography (unit: m) averaged between 29.5°N and 31.5°N over the studying period from 0630T00Z to 0705T23Z. Here the black line indicates the observation, the red line for UM-2p2, the blue one for UM-4p4 and the orange line for UM-GL. (b)–(e) are the precipitation frequency (unit: %) during the studying period: (b) observation, (c) UM-GL, (d) UM-4p4, (e) UM-2p2. The regions higher than 200.0 m are indicated by brown shadings. The rectangle denotes the main rainfall center and the black dot indicates Wuhan city. The small green rectangle indicates the small mountain region (114.5°E~117.5°E, 29.5°N~31.5°N)

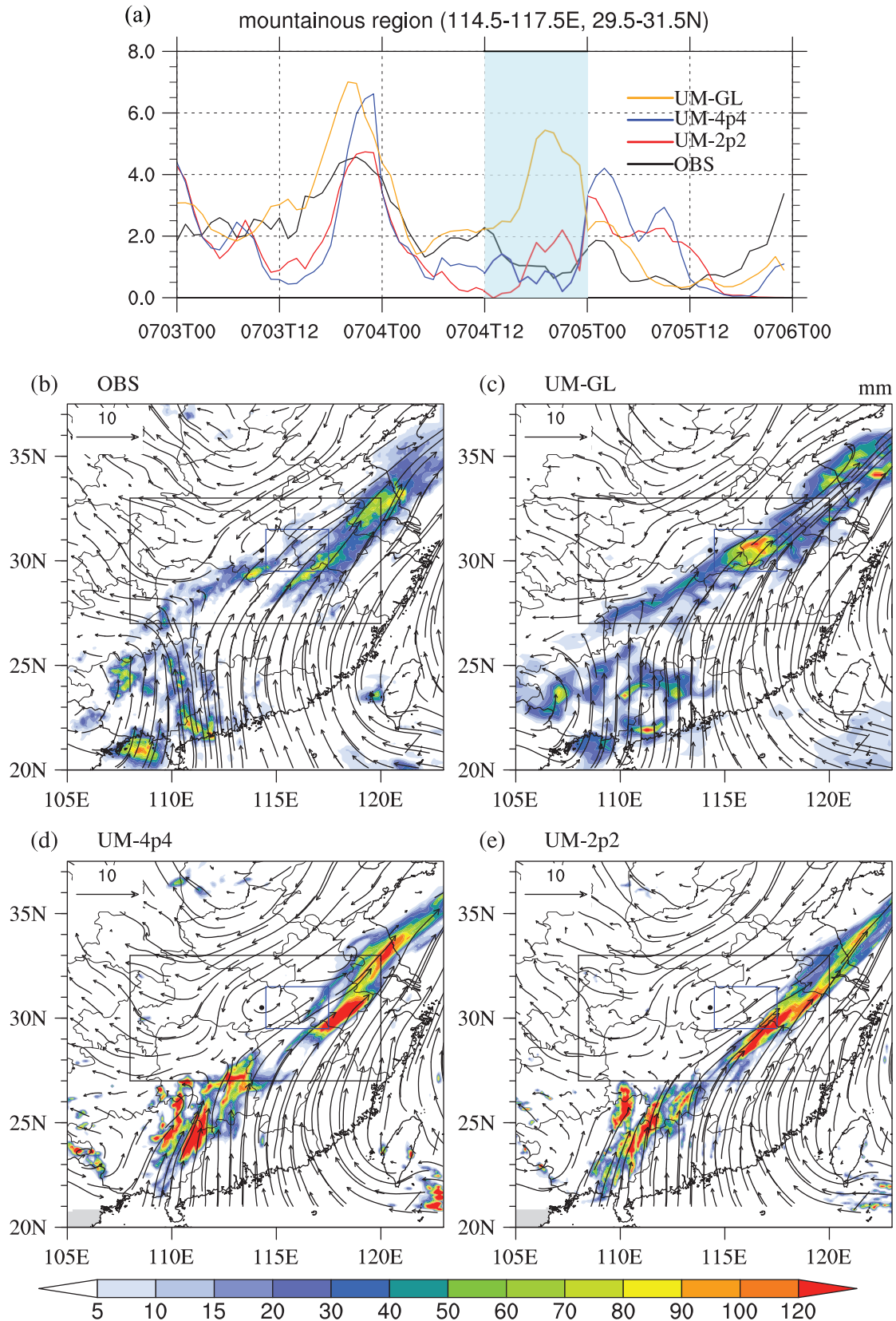


FIGURE 11 (a) Time series of hourly precipitation rates (mm/hr) over the small mountain region ($114.5^{\circ}\text{E}\sim 117.5^{\circ}\text{E}$, $29.5^{\circ}\text{N}\sim 31.5^{\circ}\text{N}$), during the time period from 0703T00Z to 0705T23Z. Here the black line indicates the observation, the red line for UM-2p2, the blue one for UM-4p4 and the orange line for UM-GL. A short time period from 0704T12Z to 0705T00Z are indicated by the light blue shadow; (b)–(e) are the accumulated rainfall (shading; unit: mm) from 0704T12Z to 0705T00Z and the low-level (850 hPa) associated atmospheric circulations (vectors). The big black rectangle denotes the main rainfall center and the small blue rectangle indicates the small mountain region

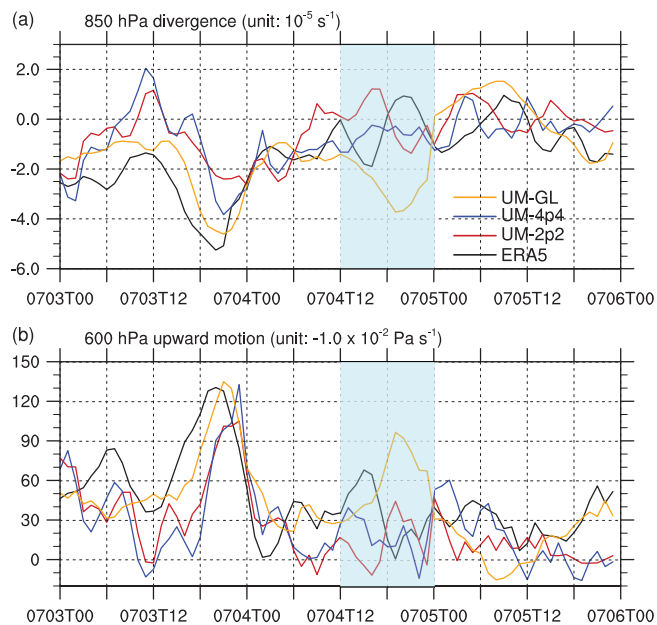


FIGURE 12 Time series of hourly (a) 850 hPa divergence (unit: 10^{-5} s^{-1}) and (b) 600 hPa upward motion (unit: $-1.0 \times 10^{-2} \text{ Pa/s}$) over the small mountain region ($114.5^{\circ}\text{E} \sim 117.5^{\circ}\text{E}$, $29.5^{\circ}\text{N} \sim 31.5^{\circ}\text{N}$), during the time period from 0703T00Z to 0705T23Z. Here the black line indicates the observation, the red line for UM-2p2, the blue one for UM-4p4 and the orange line for UM-GL. A short time period from 0704T12Z to 0705T00Z are indicated by the light blue shadow

observed. For example, we have investigated how the CPMs do a much better job in simulating a narrow heavy rainfall center from 0704T12Z to 0705T00Z. Finally, CPMs give a much better representation of orographic precipitation than the global model, perhaps due to their ability to organize convection into narrow heavy rainfall center before these interact with the local topography.

4.2 | Discussion

We may speculate as to the importance of the above results for two applications: firstly, for short-range (e.g., 13–36 hr) predictions of heavy rainfall over the Yangtze River Valley; secondly, the potential for CPMs to improve on global model simulations. Although these conclusions are necessarily speculative, at this stage, it is noteworthy that: (a) CPMs may be needed to capture the effects of the complex topography of the Yangtze River Valley on rainfall; (b) although the CPM used here is better able to produce heavy (40.0–90.0 mm/day) rain rates in this heavy rainfall case, there is a tendency for heavy rainfall to be too intense in CPMs (see Figure 8b,c); (c) we found no large benefits in the predicting of track or strength of the large-scale southwest vortex and also time series of hourly precipitation averaged over main rainfall center by using CPMs, which means that the global model (25 km) already has the ability to reproduce such kind of large-scale circulation, but on the other hand,

CPMs are needed for simulating the coherent west-to-east propagating small-scale features within the rain-belt associated with the LLV during P1 (Figure 3c,d) and also reduce the spurious topographical rainfall simulated by UM-GL; (d) convective organization, e.g., the ability of the model to produce the narrow heavy rainfall corridor within the Mei-yu front, is improved by the CPMs (see Figure 11); (e) The model performance of UM-4p4 and UM-2p2 is broadly comparable, further increasing model horizontal resolution from 4.4 to 2.2 km gives very little added value. This implies that the principle difference between CPMs and global simulations mainly comes from different representation of convection (i.e., explicit versus parameterization), and model horizontal resolution of 4.4 km is adequate for reproducing this kind of heavy precipitation event.

In this study, we have used only the 13–36 hr of each simulation for analysis, which is consistent with the previous study of this event (Li *et al.*, 2018). The full 6-days of each simulation may be exploited in a later study, focusing on other scientific topics (for example, short-range forecast skill and effects of different initialized time). Also, more sensitivity tests will be performed in the future work, focusing on the impact of different physical process (such as planetary boundary layer and cloud microphysics). In addition, further investigation on the added values of CPMs for the aforementioned factors over eastern China during the warm season is a useful topic of future work.

ACKNOWLEDGEMENTS

This work was jointly supported by the National Natural Science Foundation of China under grant No. (41420104006, 41330423) and Climate Science for Service Partnership: China. Kalli Furtado and Sean Milton were funded by the UK-China Research & Innovation Partnership Fund through the Met Office Climate Science for Service Partnership (CSSP) China as part of the Newton Fund.

ORCID

Puxi Li  <https://orcid.org/0000-0002-4812-2184>

REFERENCES

- Ban, N., Schmidli, J. and Schär, C. (2014) Evaluation of the convection-resolving regional climate modeling approach in decade-long simulations. *Journal of Geophysical Research*, 119(13), 7889–7907. <https://doi.org/10.1002/2014JD021478>.
- Bernardet, L.R., Grasso, L.D., Nachamkin, J.E., Finley, C.A. and Cotton, W.R. (2000) Simulating convective events using a high-resolution mesoscale model. *Journal of Geophysical Research*, 105(D11), 14963–14982.
- Boutle, I.A., Abel, S.J., Hill, P.G. and Morcrette, C.J. (2014) Spatial variability of liquid cloud and rain: observations and microphysical effects. *Quarterly Journal of the Royal Meteorological Society*, 140(679), 583–594. <https://doi.org/10.1002/qj.2140>.

- Boyle, J., Klein, S., Zhang, G., Xie, S. and Wei, X. (2008) Climate model forecast experiments for TOGA COARE. *Monthly Weather Review*, 136(3), 808–832.
- Chen, G., Sha, W., Iwasaki, T. and Wen, Z. (2017) Diurnal cycle of a heavy rainfall corridor over East Asia. *Monthly Weather Review*, 145(8), 3365–3389.
- Chen, S.J., Kuo, Y.H., Wang, W., Tao, Z. and Cui, B. (1998) A modeling case study of heavy rainstorms along the Mei-Yu front. *Monthly Weather Review*, 126(9), 2330–2351.
- Clark, A.J., Gallus, W.A., Jr., Xue, M. and Kong, F. (2009) A comparison of precipitation forecast skill between small convection-allowing and large convection-parameterizing ensembles. *Weather and Forecasting*, 24(4), 1121–1140.
- Dai, A., Giorgi, F. and Trenberth, K.E. (1999) Observed and model-simulated diurnal cycles of precipitation over the contiguous United States. *Journal of Geophysical Research*, 104(D6), 6377–6402.
- Dee, D.P., Uppala, S.M., Simmons, A.J., Berrisford, P., Poli, P., Kobayashi, S., Andrae, U., Balmaseda, M.A., Balsamo, G., Bauer, P., Bechtold, P., Beljaars, A.C.M., van de Berg, L., Bidlot, J., Bormann, N., Delsol, C., Dragani, R., Fuentes, M., Geer, A.J., Haimberger, L., Healy, S.B., Hersbach, H., Hólm, E.V., Isaksen, L., Kallberg, P., Köhler, M., Matricardi, M., McNally, A.P., Monge-Sanz, B.M., Morcrette, J.-J., Park, B.-K., Peubey, C., de Rosnay, P., Tavolato, C., Thépaut, J.-N. and Vitart, F. (2011) The ERA-interim reanalysis: configuration and performance of the data assimilation system. *Quarterly Journal of the Royal Meteorological Society*, 137, 553–597. <https://doi.org/10.1002/qj.828>.
- Ding, Y. (1992) Summer monsoon rainfalls in China. *Journal of the Meteorological Society of Japan. Series II*, 70, 373–396.
- Ding, Y. and Chan, J.C. (2005) The East Asian summer monsoon: an overview. *Meteorology and Atmospheric Physics*, 89(1–4), 117–142. <https://doi.org/10.1007/s00703-005-0125-z>.
- Doswell, C.A., Brooks, H.E. and Maddox, R.A. (1996) Flash flood forecasting: an ingredients-based methodology. *Weather and Forecasting*, 11(4), 560–581.
- Fosser, G., Khodayar, S. and Berg, P. (2015) Benefit of convection permitting climate model simulations in the representation of convective precipitation. *Climate Dynamics*, 44(1–2), 45–60.
- Furtado, K., Field, P.R., Cotton, R. and Baran, A.J. (2015) The sensitivity of simulated high clouds to ice crystal fall speed, shape and size distribution. *Quarterly Journal of the Royal Meteorological Society*, 141(690), 1546–1559. <https://doi.org/10.1002/qj.2457>.
- Gregory, D. and Rowntree, P.R. (1990) A mass flux convection scheme with representation of cloud ensemble characteristics and stability-dependent closure. *Monthly Weather Review*, 118(7), 1483–1506.
- Holloway, C.E., Woolnough, S.J. and Lister, G.M. (2013) The effects of explicit versus parameterized convection on the MJO in a large-domain high-resolution tropical case study. Part I: characterization of large-scale organization and propagation. *Journal of the Atmospheric Sciences*, 70(5), 1342–1369.
- Holloway, C.E., Woolnough, S.J. and Lister, G.M. (2015) The effects of explicit versus parameterized convection on the MJO in a large-domain high-resolution tropical case study. Part II: processes leading to differences in MJO development. *Journal of the Atmospheric Sciences*, 72(7), 2719–2743.
- Iyer, E.R., Clark, A.J., Xue, M. and Kong, F. (2016) A comparison of 36–60 hour forecasts from convection-allowing and convection-parameterizing ensembles. *Weather and Forecasting*, 31(2), 647–661.
- Jiang, Z., Zhang, D.L., Xia, R. and Qian, T. (2017) Diurnal variations of presummer rainfall over southern China. *Journal of Climate*, 30(2), 755–773.
- Joyce, R.J., Janowiak, J.E., Arkin, P.A. and Xie, P. (2004) Cmorph: a method that produces global precipitation estimates from passive microwave and infrared data at high spatial and temporal resolution. *Journal of Hydrometeorology*, 5(3), 487–503.
- Kendon, E.J., Ban, N., Roberts, N.M., Fowler, H.J., Roberts, M.J., Chan, S.C., Evans, J.P., Fosser, G. and Wilkinson, J.M. (2017) Do convection-permitting regional climate models improve projections of future precipitation change? *Bulletin of the American Meteorological Society*, 98(1), 79–93.
- Kendon, E.J., Roberts, N.M., Senior, C.A. and Roberts, M.J. (2012) Realism of rainfall in a very high-resolution regional climate model. *Journal of Climate*, 25(17), 5791–5806.
- Klein, S.A., Jiang, X., Boyle, J., Malyshev, S. and Xie, S. (2006) Diagnosis of the summertime warm and dry bias over the U.S. southern great plains in the GFDL climate model using a weather forecasting approach. *Geophysical Research Letters*, 33(18), L18805. <https://doi.org/10.1029/2006GL027567>.
- Lean, H.W., Clark, P.A., Dixon, M., Roberts, N.M., Fitch, A., Forbes, R. and Halliwell, C. (2008) Characteristics of high-resolution versions of the met office unified model for forecasting convection over the United Kingdom. *Monthly Weather Review*, 136(9), 3408–3424.
- Li, J., Chen, H., Rong, X., Su, J., Xin, Y., Furtado, K., Milton, S. and Li, N. (2018) How well can a climate model simulate an extreme precipitation event: a case study using the transpose-AMIP experiment. *Journal of Climate*, 31(16), 6543–6556.
- Liu, H., Zhang, D.L. and Wang, B. (2008) Daily to submonthly weather and climate characteristics of the summer 1998 extreme rainfall over the Yangtze River Basin. *Journal of Geophysical Research*, 113, D22101. <https://doi.org/10.1029/2008JD010072>.
- Liu, H., Zhang, D.L. and Wang, B. (2010) Impact of horizontal resolution on the regional climate simulations of the summer 1998 extreme rainfall along the Yangtze River Basin. *Journal of Geophysical Research*, 115, D12115. <https://doi.org/10.1029/2009JD012746>.
- Lock, A.P., Brown, A.R., Bush, M.R., Martin, G.M. and Smith, R.N.B. (2000) A new boundary layer mixing scheme. Part I: scheme description and single-column model tests. *Monthly Weather Review*, 128(9), 3187–3199.
- Luo, Y. and Chen, Y. (2015) Investigation of the predictability and physical mechanisms of an extreme-rainfall-producing mesoscale convective system along the Meiyu front in east China: an ensemble approach. *Journal of Geophysical Research*, 120(20), 10593–10618. <https://doi.org/10.1002/2015JD023584>.
- Luo, Y., Gong, Y. and Zhang, D.L. (2014) Initiation and organizational modes of an extreme-rain-producing mesoscale convective system along a Mei-Yu front in East China. *Monthly Weather Review*, 142(1), 203–221.
- Luo, Y., Wang, H., Zhang, R., Qian, W. and Luo, Z. (2013) Comparison of rainfall characteristics and convective properties of monsoon precipitation systems over south China and Yangtze and Huai River Basin. *Journal of Climate*, 26(1), 110–132.
- Molinari, J. and Dudek, M. (1992) Parameterization of convective precipitation in mesoscale numerical models: a critical review. *Monthly Weather Review*, 120(2), 326–344.

- Ninomiya, K. (1984) Characteristics of Baiu front as a predominant subtropical front in the summer Northern Hemisphere. *Journal of the Meteorological Society of Japan*, 62, 880–894.
- Ninomiya, K. and Shibagaki, Y. (2007) Multi-scale features of the Meiyu-Baiu front and associated precipitation systems. *Journal of the Meteorological Society of Japan. Series II*, 85, 103–122.
- Pan, Y., Shen, Y., Yu, Q.Q. and Zhao, P. (2012) Merged analyses of gauge-satellite hourly precipitation over China based on OI technique (in Chinese with English abstract). *Acta Meteorologica Sinica*, 70(6), 1381–1389.
- Phillips, T.J., Potter, G.L., Williamson, D.L., Cederwall, R.T., Boyle, J.S., Fiorino, M., Hnilo, J.J., Olson, J.G., Xie, S. and Yio, J.J. (2004) Evaluating parametrizations in general circulation models: climate simulation meets weather prediction. *Bulletin of the American Meteorological Society*, 85, 1903–1915. <https://doi.org/10.1175/BAMS-85-12-1903>.
- Prein, A.F., Langhans, W., Fossier, G., Ferrone, A., Ban, N., Goergen, K., Keller, M., Tolle, M., Gutjahr, O., Feser, F., Brisson, E., Kollet, S., Schmidli, J., Van Lipzig, N.P.M. and Leung, R. (2015) A review on regional convection-permitting climate modeling: demonstrations, prospects, and challenges. *Reviews of Geophysics*, 53(2), 323–361. <https://doi.org/10.1002/2014RG000475>.
- Roberts, N.M. and Lean, H.W. (2008) Scale-selective verification of rainfall accumulations from high-resolution forecasts of convective events. *Monthly Weather Review*, 136(1), 78–97.
- Sampe, T. and Xie, S.P. (2010) Large-scale dynamics of the Meiyu-Baiu rainband: environmental forcing by the westerly jet. *Journal of Climate*, 23(1), 113–134.
- Schwartz, C.S., Kain, J.S., Weiss, S.J., Xue, M., Bright, D.R., Kong, F., Thomas, K.W., Levit, J.J. and Coniglio, M.C. (2009) Next-day convection-allowing WRF model guidance: a second look at 2-km versus 4-km grid spacing. *Monthly Weather Review*, 137(10), 3351–3372. <https://doi.org/10.1175/2009MWR2924.1>.
- Shen, Y., Zhao, P., Pan, Y. and Yu, J. (2014) A high spatiotemporal gauge-satellite merged precipitation analysis over China. *Journal of Geophysical Research*, 119(6), 3063–3075. <https://doi.org/10.1002/2013JD020686>.
- Shinoda, T., Uyeda, H. and Yoshimura, K. (2005) Structure of moist layer and sources of water over the southern region far from the Meiyu/Baiu front. *Journal of the Meteorological Society of Japan. Series II*, 83(2), 137–152.
- Smith, R.N.B. (1990) A scheme for predicting layer clouds and their water content in a general circulation model. *The Quarterly Journal of the Royal Meteorological Society*, 116(492), 435–460. <https://doi.org/10.1002/qj.49711649210>.
- Sun, J., Zhao, S., Xu, G. and Meng, Q. (2010) Study on a mesoscale convective vortex causing heavy rainfall during the Mei-yu season in 2003. *Advances in Atmospheric Sciences*, 27(5), 1193–1209.
- Tao, S.Y. (1987) A review of recent research on the East Asian summer monsoon in China. *China, Monsoon Meteorology*, 60–92.
- Tomita, T., Yamaura, T. and Hashimoto, T. (2011) Interannual variability of the Baiu season near Japan evaluated from the equivalent potential temperature. *Journal of the Meteorological Society of Japan. Series II*, 89(5), 517–537.
- Walters, D.N., Brooks, M., Boutle, I., Melvin, T., Stratton, R., Wells, H., Williams, K., Bushell, A., Copsey, D., Earnshaw, P., Edwards, J., Gross, M., Hardiman, S., Harris, C., Heming, J., Klingaman, N., Levine, R., Manners, J., Martin, G., Milton, S., Mittermaier, M., Morcretter, C., Riddick, T., Roberts, M., Sanchez, C., Selwood, P., Smith, C., Tennant, W., Vosper, S., Vidale, P.L., Wilkinson, J., Wood, N., Woolnough, S. and Xavier, P. (2016) The Met Office Unified Model Global Atmosphere 6.0/6.1 and JULES Global Land 6.0/6.1 configurations. *Geoscientific Model Development*, 10(4), 1487–1520.
- Wang, W.C., Gong, W. and Wei, H. (2000) A regional model simulation of the 1991 severe precipitation event over the Yangtze-Huai River Valley. Part I: precipitation and circulation statistics. *Journal of Climate*, 13(1), 74–92.
- Weusthoff, T., Ament, F., Arpagaus, M. and Rotach, M.W. (2010) Assessing the benefits of convection permitting models by fuzzy Verification-examples from MAP D-PHASE. *Monthly Weather Review*, 138(9), 3418–3433.
- Wilkinson, J.M. (2017) A technique for verification of convection-permitting NWP model deterministic forecasts of lightning activity. *Weather and Forecasting*, 32(1), 97–115. <https://doi.org/10.1175/WAF-D-16-0106.1>.
- Williams, K.D., Bodas-Salcedo, A., Deque, M., Fermepin, S., Medeiros, B., Wanatabe, M., Jakob, C., Klein, S.A., Senior, C.A. and Williamson, D.L. (2013) The transpose-AMIP II experiment and its application to the understanding of southern ocean cloud biases in climate models. *Journal of Climate*, 26(10), 3258–3274. <https://doi.org/10.1175/JCLI-D-12-00429.1>.
- Williamson, D.L., Boyle, J., Cederwall, R., Fiorino, M., Hnilo, J., Olson, J., Phillips, T., Potter, G. and Xie, S.C. (2005) Moisture and temperature balances at the atmospheric radiation measurement Southern Great Plains Site in forecasts with the community atmosphere model (CAM2). *Journal of Geophysical Research*, 110, D15S16. <https://doi.org/10.1029/2004JD005109>.
- Williamson, D.L. and Olson, J.G. (2007) A comparison of forecast errors in CAM2 and CAM3 at the ARM Southern Great Plains Site. *Journal of Climate*, 20(20), 4572–4585.
- Wilson, D.R. and Ballard, S.P. (1999) A microphysically based precipitation scheme for the UK meteorological office unified model. *The Quarterly Journal of the Royal Meteorological Society*, 125(557), 1607–1636. <https://doi.org/10.1002/qj.49712555707>.
- Wood, N., Staniforth, A., White, A., Allen, T., Diamantakis, M., Gross, M., Melvin, T., Smith, C., Vosper, S., Zerroukat, M. and Thuburn, J. (2013) An inherently mass-conserving semi-implicit semi-Lagrangian discretization of the deep-atmosphere global non-hydrostatic equations. *Quarterly Journal of the Royal Meteorological Society*, 140, 1505–1520. <https://doi.org/10.1002/qj.2235>.
- Wu, R.G., Hu, Z.Z. and Kirtman, B.P. (2003) Evolution of ENSO-related rainfall anomalies in East Asia. *Journal of Climate*, 16, 3742–3758.
- Xu, W., Zipser, E.J. and Liu, C. (2009) Rainfall characteristics and convective properties of Mei-yu precipitation systems over South China, Taiwan, and the South China Sea. Part I: TRMM observations. *Monthly Weather Review*, 137(12), 4261–4275.
- Xue, M., Kong, F.Y., Thomas, K.W., Gao, J.D., Wang, Y.H., Brewster, K.A. and Droegemeier, K.K. (2013) Prediction of convective storms at convection-resolving 1 km resolution over continental United States with radar data assimilation: an example case of 26 May 2008 and precipitation forecasts from spring 2009. *Advances in Meteorology*, 2013, 259052. <https://doi.org/10.1155/2013/259052>.
- Yu, R., Xu, Y., Zhou, T. and Li, J. (2007a) Relation between rainfall duration and diurnal cycle in the warm season precipitation over central eastern China. *Geophysical Research Letters*, 34(13), 173–180. <https://doi.org/10.1029/2007GL030315>.
- Yu, R., Zhou, T., Xiong, A., Zhu, Y. and Li, J. (2007b) Diurnal variation of summer precipitation over contiguous China. *Geophysical*

- Research Letters*, 34(1), 223–234. <https://doi.org/10.1029/2006GL028129>.
- Zhang, D.L., Hsie, E.Y. and Moncrieff, M.W. (1988) A comparison of explicit and implicit predictions of convective and stratiform precipitating weather systems with a meso- β -scale numerical model. *Quarterly Journal of the Royal Meteorological Society*, 114(479), 31–60.
- Zhang, D.L., Kain, J.S., Fritsch, J.M. and Gao, K. (1994) Comments on “parameterization of convective precipitation in mesoscale numerical models: a critical review”. *Monthly Weather Review*, 122(9), 2222–2231.
- Zhou, C., Wang, K. and Qi, D. (2018) Attribution of the July 2016 extreme precipitation event over China's Wuhang. *Bulletin of the American Meteorological Society*, 99(1), S107–S112.
- Zhou, T., Gong, D., Li, J. and Li, B. (2009) Detecting and understanding the multi-decadal variability of the East Asian Summer Monsoon recent progress and state of affairs. *Meteorologische Zeitschrift*, 18(4), 455–467.
- Zhou, T., Yu, R., Chen, H., Dai, A. and Pan, Y. (2008) Summer precipitation frequency, intensity, and diurnal cycle over China: a comparison of satellite data with rain gauge observations. *Journal of Climate*, 21, 3997–4010.

How to cite this article: Li P, Guo Z, Furtado K, *et al.* Prediction of heavy precipitation in the eastern China flooding events of 2016: Added value of convection-permitting simulations. *QJR Meteorol Soc.* 2019;145:3300–3319. <https://doi.org/10.1002/qj.3621>